Focusing of high polarization order axially-symmetric polarized beams

Zhehai Zhou (周哲海)[1,2*], Qiaofeng Tan (谭峭峰)[1], and Guofan Jin (金国藩)[1]

[1] *State Key Laboratory of Precision Measurement Technology and Instruments, Tsinghua University, Beijing 100084, China*

[2] *Department of Optical Information Science & Technology, Beijing Information Science & Technology University, Beijing 100192, China*

[*] *E-mail: zhouzh07@mails.tsinghua.edu.cn*

Received October 29, 2008

We study the high numerical aperture focusing properties and typical applications of axially-symmetric polarized beams (ASPBs) with high polarization orders. We calculate the field distribution near focus of an aplanatic system for incident ASPBs with different polarization orders and initial azimuthal angles, and based on the simulation results, we find some unique focusing properties of the beams, such as ever on-axis energy null, strong longitudinal field, and flowerlike intensity distribution at focus. In addition, we can manipulate the three-dimensional (3D) focused field distribution flexibly by use of diffractive optical elements (DOEs), which will give rise to some interesting applications, and we also discuss possible applications and present an example of a 3D optical chain at last.

OCIS codes: 110.2990, 260.5430, 140.3300.

doi: 10.3788/COL20090710.0938.

In past several years, many researches on axially-symmetric polarized beams (ASPBs) have drawn considerable attention, especially on radially polarized beams and azimuthally polarized beams for their special applications in lithography, particle trapping, electron acceleration, material processing, scanning microscopy, tight focusing, and data storage[1−7]. Many progresses have been made in terms of the formation methods, high numerical aperture focusing properties, and practical applications. But to the best of our knowledge, the research on axially-symmetric polarized beams with higher polarization orders has not been thoroughly carried on, and their applications have also not been fully exploited. In the letter, we study the high numerical aperture (NA) focusing properties of such beams. We derive the mathematical expressions for the focusing fields, show the focusing field distributions near focus, and discuss some possible applications.

For an ASPB, as shown in Fig. 1, the polarization orientation angle $\Phi(r,\ \phi)$ of the electric field only depends on the azimuthal angle ϕ as $\Phi(r,\ \phi)=P\times\phi+\phi_0$, where P is the polarization order number, ϕ is the azimuthal angle of the polar coordinate system, and ϕ_0 is the initial polarization orientation for ϕ=0. Obviously, radially polarized beams ($P=1$, $\phi_0=0$) and azimuthally polarized beams ($P=1$, $\phi_0=\pi/2$) are $P=1$ ASPBs.

Figure 2 illustrates the geometry of the problem. Here, we adopt the similar notation used by Richards *et al.*[8]. The incident field is an ASPB, which is assumed to have planar phase front. f is the focal length of the objective lens, $S(r_{\rm S},\ \phi_{\rm S},\ z_{\rm S})$ is an observation point near the focal plane, $\phi_{\rm s}$ denotes the azimuthal angle with respect to the x-axis, and θ represents the polar angle.

Following the theory of Richards *et al.*[8] and Youngworth *et al.*[9], the focal field of an ASPB can be written as

$$\begin{aligned}
E_{\rm r} &= \frac{-{\rm i}A}{\pi}\int_{\theta_{\min}}^{\theta_{\max}}\int_0^{2\pi} l(\theta)\sin\theta\sqrt{\cos\theta}\,{\rm e}^{{\rm i}k[z_{\rm s}\cos\theta+r_{\rm s}\sin\theta\cos(\phi-\phi_{\rm s})]}\cos\left[(P-1)\phi+\phi_0\right]\cos\theta\cos(\phi-\phi_{\rm s}){\rm d}\theta{\rm d}\phi,\\
E_{\phi} &= \frac{-{\rm i}A}{\pi}\int_{\theta_{\min}}^{\theta_{\max}}\int_0^{2\pi} l\left(\theta\right)\sin\theta\sqrt{\cos\theta}\,{\rm e}^{{\rm i}k[z_{\rm s}\cos\theta+r_{\rm s}\sin\theta\cos(\phi-\phi_{\rm s})]}\sin\left[(P-1)\,\phi+\phi_0\right]\cos\left(\phi-\phi_{\rm s}\right){\rm d}\theta{\rm d}\phi,\\
E_{\rm z} &= \frac{-{\rm i}A}{\pi}\int_{\theta_{\min}}^{\theta_{\max}}\int_0^{2\pi} l\left(\theta\right)\sin\theta\sqrt{\cos\theta}\,{\rm e}^{{\rm i}k[z_{\rm s}\cos\theta+r_{\rm s}\sin\theta\cos(\phi-\phi_{\rm s})]}\cos\left[(P-1)\,\phi+\phi_0\right]\sin\theta{\rm d}\theta{\rm d}\phi,
\end{aligned}\tag{1}$$

where $E_{\rm r}$, E_{ϕ}, and $E_{\rm z}$ are the amplitudes of the three orthogonal components, $l\left(\theta\right)$ is the pupil apodization function, which denotes the relative amplitude and phase of the field, k is the wavelength number, $\theta_{\max}$ and $\theta_{\min}$ are the maximal polar angle and the minimal polar angle determined by the NA of the objective lens.

Based on Eq. (1), we calculate the focusing field distribution of different ASPBs, but only present the results for $P=4$ as typical examples because of the limited length requirement. In our numerical examples, a simple pupil apodization function is adopted as

$$l\left(\theta\right)=\begin{cases}1 & 0\le\theta\le\theta_{\max}\\ 0 & \text{otherwise}\end{cases},\tag{2}$$

where $\theta_{\max}=\sin^{-1}\left({\rm NA}/n\right)$, n is the index of refraction, and θ_{min} is set to be 0. For all examples in the letter, n is set to be 1, and all length measurements are in units of wavelengths, therefore, $\lambda=1$. The amplitude A is also assumed to be 1.

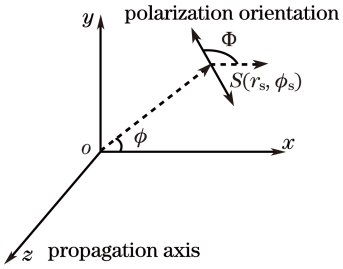

Fig. 1. Polarization orientation of an ASPB.

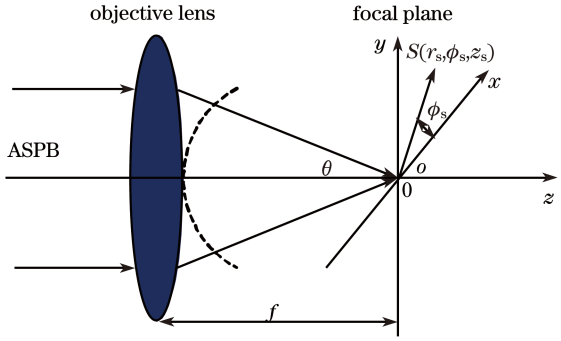

Fig. 2. Focusing of an ASPB.

Figure 3 shows the intensity $I = |E|^2$ of the three orthogonal components and total field for ϕ_0=0° at focus (x-y plane) and through focus (r-z plane) with P=4, NA=0.95. And the intensity distribution of the total field at focus for different NAs is also shown in Fig. 4 in order to present the focusing properties clearly. The on-axis energy null and annular intensity distribution are apparent. In addition, the intensity at focus (x-y plane) presents flowerlike distribution with the increase of NA. The number of the lobes is $2 \times (P-1)$.

Meanwhile, the longitudinal field is stronger than the transverse field (the sum of the azimuthal component and the radial component). This trend is shown in Fig. 5, which displays the plot for the ratio of the maximum intensities of the longitudinal and transverse fields versus the NA of the lens with $P = 4$. If NA is larger than 0.78, the longitudinal field I_z will be stronger than the transverse field I_r. When NA is close to 1, the ratio approaches 3. If adopting the appropriate pupil apodization function $l(\theta)$, we can increase the ratio further, which is desirable for some applications such as electron acceleration and near-field microscopy.

If the polarization order number P and initial azimuthal angle ϕ_0 are changed, the intensity distribution of the three orthogonal components and the total field will also change. Figure 6 shows the total field with $P = 5$, NA $= 0.95$, $\phi_0 = 0$, and $\phi_0 = \pi/4$, respectively. The flowerlike intensity distribution will remain, the number of lobes is still $2 \times (P-1)$, but the lobes will rotate if ϕ_0 changes, and the rotation angle is ϕ_0.

Compared with radially polarized beams and azimuthally polarized beams (P=1), ASPBs with higher polarization order number P are distinguished by the on-axis energy null and the flowerlike intensity distribution near focus, and the number of lobes is related with P as $2 \times (P-1)$. With the increase of NA, the longitudinal field is stronger than the transverse field. Through changing ϕ_0, the field will be easily rotated. These unique characteristics may be useful in applications such as electron acceleration, particle trapping, near-field microscopy, material processing, and so on.

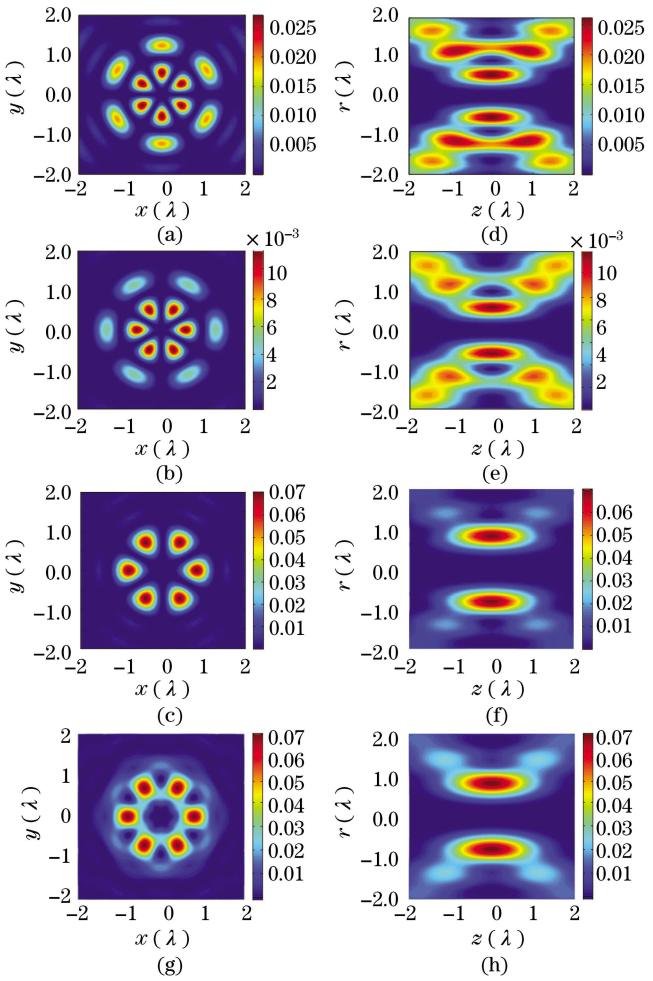

Fig. 3. Intensity distribution of three orthogonal components E_ϕ(a, d), E_r(b, e), E_z(c, f) and total field (g, h) at focus (x-y plane) and through focus (r-z plane) with P=4, ϕ_0=0.

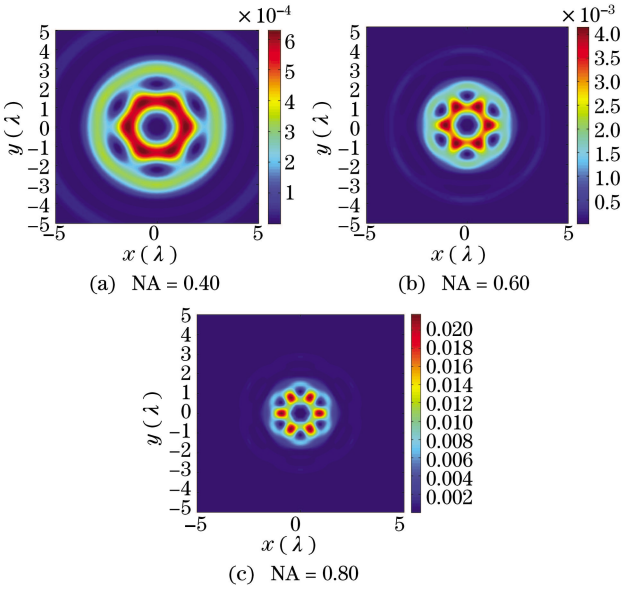

Fig. 4. Intensity distribution of the total field at focus for different NAs with P=4, ϕ_0=0.

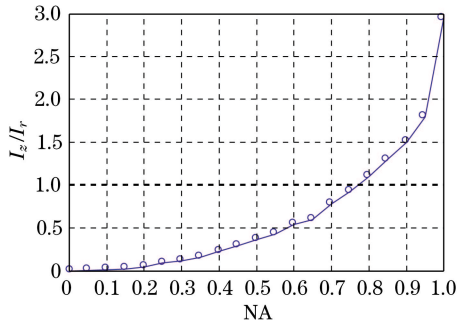

Fig. 5. Ratio of the maximum intensities of the longitudinal and transverse fields versus the NA of the lens.

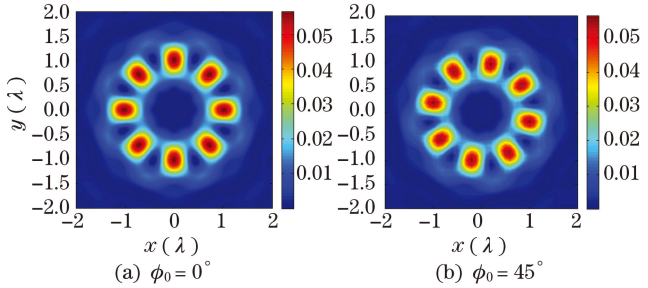

Fig. 6. Intensity distribution of the total field at focus (x-y plane) with P=5, NA=0.95.

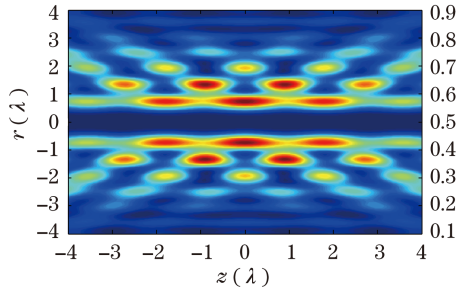

Fig. 7. Normalized intensity distribution of the total field near the focus.

The three-dimensional (3D) optical chain can stably trap and deliver multiple individual particles in three dimensions at different planes near the focus[10]. We use a diffractive optical element (DOE) similar to the one in Ref. [10] to generate a 3D optical chain in a high-NA focusing system, where the incident beam is an ASPB with P=4. The transmission function of the DOE is expressed as

$$T(\theta) = \begin{cases} \exp(\mathrm{i}\varphi_1) & \text{if } \theta \in [0, 0.4 \times \theta_{\max}] \\ 0 & \text{if } \theta \in [0.4 \times \theta_{\max}, 0.9 \times \theta_{\max}] \\ \exp(\mathrm{i}\varphi_3) & \text{if } \theta \in [0.9 \times \theta_{\max}, \theta_{\max}] \end{cases} . \tag{3}$$

Figure 7 shows the normalized intensity distribution of the total field through focus, where $\Delta\varphi$=φ_3−φ_1=0. The field appears like a chain along the longitudinal direction with on-axis energy null. Particles with different refractive indices (lower or higher than that of the ambient) can be trapped in different nodes (dark or bright regions) of the stack simultaneously. Different from that formed in Ref. [10], the chain is a multi-layer and annular structure. By varying $\Delta\varphi$, the chain moves along the z direction, and changing ϕ_0, the chain rotates along the azimuthal direction.

In fact, we can use the DOE to control 3D field distribution of ASPBs near focus more freely, just as the above mentioned example of the 3D optical chain. With appropriate definitions of the cost function, we can obtain different focusing field strength distribution to meet the requirements for different applications, such as flat-top beam shaping, ultra small focus with extended depth of focus, and so on.

This work was supported by the National Basic Research Program of China (No. 2007CB935303).

References

1. K. Watanabe, N. Horiguchi, and H. Kano, Appl. Opt. **46,** 4985 (2007).
2. W. Chen and Q. Zhan, Opt. Express **15,** 4106 (2007).
3. W. Chen and Q. Zhan, Chin. Opt. Lett. **5,** 709 (2007).
4. K. B. Rajesh and P. M. Anbarasam, Chin. Opt. Lett. **6,** 785 (2008).
5. S. Quabis, R. Dorn, M. Eberler, O. Glöckl, and G. Leuchs, Opt. Commun. **179,** 1 (2000).
6. T. A. Nieminen, N. R. Heckenberg, and H. Rubinsztein-Dunlop, Opt. Lett. **33,** 122 (2008).
7. W.-C. Kim, N.-C. Park, Y.-J. Yoon, H. Choi, and Y.-P. Park, Opt. Rev. **14,** 236 (2007).
8. B. Richards and E. Wolf, Proc. Roy. Soc. A **253,** 358 (1959).
9. K. S. Youngworth and T. G. Brown, Opt. Express **7,** 77 (2000).
10. Y. Zhao, Q. Zhan, Y. Zhang, and Y.-P. Li, Opt. Lett. **30,** 848 (2005).